Chaos and Localization on 1-dimensional Nonlinear Disordered Lattices

Ioannis Gkolias[1], Haris Skokos[2]

Physics Department, Aristotle University of Thessaloniki, Thessaloniki, GR54124 Greece

Sergej Flach[3]

New Zealand Institute for Advanced Study, Centre for Theoretical Chemistry and Physics, Massey University, Auckland, New Zealand

emails : [1]igkoli@physics.auth.gr, [2]hskokos@auth.gr, [3]s.flach@massey.ac.nz

1. Abstract

Nonlinear waves destroy Anderson localization in disordered potentials. Computational studies yield a subdiffusive wave packet spreading, as also confirmed in experiments. Theoretical explanations are based on chaotic dynamics assumptions necessary for phase decoherence and delocalization. We follow the wave packet dynamics and compute the time dependence of chaos indicators - Lyapunov exponents and deviation vector distributions. Chaotic dynamics is observed. It does not cross over into regular dynamics. Chaos time scales stay shorter than the time scales of slow wave packet spreading, allowing for complete thermalization of the packet. Chaotic spots meander through the wave packet in time. Therefore the previously assumed phase decoherence can persist to arbitrarily large times, leading to a complete delocalization of wave packets.

2. Model, equations and methods of analysis

The spreading of wave packets was numerically studied in a number of classes of wave equations. Here we choose for practical reasons a chain of coupled anharmonic oscillators with random harmonic frequencies which belongs to the class of quartic Klein-Gordon (KG) lattices. In a number of computational studies on wave packet spreading this model is behaving very close to Nonlinear Schrödinger equations with random potentials [2, 3, 5, 7, 8, 9, 10]. The Hamiltonian of the quartic Klein-Gordon chain (KG) of coupled anharmonic oscillators with coordinates u_l and momenta p_l is

$$\mathcal{H}_K = \sum_l \frac{p_l^2}{2} + \frac{\tilde{\epsilon}_l}{2}u_l^2 + \frac{1}{4}u_l^4 + \frac{1}{2W}(u_{l+1}-u_l)^2 \ . \qquad (1)$$

The equations of motion are $\ddot{u}_l = -\partial\mathcal{H}_K/\partial u_l$, and $\tilde{\epsilon}_l$ are chosen uniformly from the interval $\left[\frac{1}{2},\frac{3}{2}\right]$.
We analyze normalized energy distributions $\epsilon_\nu \geq 0$ using the second moment $m_2 = \sum_l (l-\bar{l})^2\epsilon_l$ and the participation number $P = 1/\sum_l \epsilon_l^2$, which measures the number of the strongest excited sites in ϵ_ν.
During the wave packet evolution we further estimate the maximum Lyapunov exponent (mLE) Λ_1 as the limit for $t\to\infty$ of the quantity $\Lambda(t) = t^{-1}\ln(\|\vec{v}(t)\|/\|\vec{v}(0)\|)$, often called *finite time mLE*. $\vec{v}(0)$, $\vec{v}(t)$ are deviation vectors from the given trajectory, at times $t=0$ and $t>0$ respectively, and $\|\cdot\|$ denotes the usual vector norm [11]. In our study we also compute normalized deviation vector distributions (DVDs) $w_l = (v_l^2 + v_{l+N}^2)/\sum_l (v_l^2+v_{l+N}^2)$.
We use the symplectic integrator $SABA_2$ with corrector [12, 3] for the integration of the equations of motion, and its extension according to the so-called tangent map method [13, 14] for the integration of the variational equations. We considered lattices with $N=1000$ to $N=2000$ sites in our computations, in order to exclude finite-size effects in the evolution of the wave packets, and an integration time step $\tau = 0.2$, which kept the relative energy error always less than 10^{-4}.

3. Results

We study the evolution of trajectories in three different cases. The trajectories in this cases are known to evolve in the asymptotic regime of *'weak chaos'* [2, 3, 5].

- Case I : single site excitation with total energy $E = 0.4$ and $W = 4$
- Case II : initial energy density $\epsilon = 0.01$ distributed evenly among a block of 21 central sites for $W = 4$
- Case III : initial energy density $\epsilon = 0.01$ distributed evenly among a block of 37 central sites for $W = 3$

In *Fig. 1* we present the time evolution of m_2, P and Λ of a single trajectory of Case I.

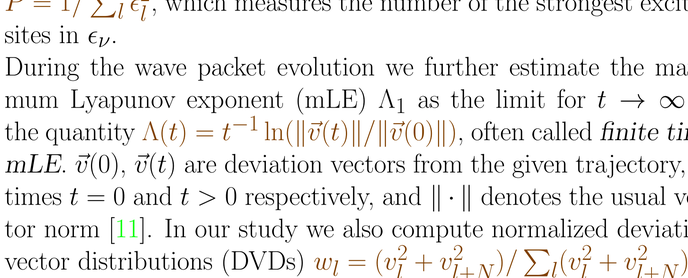

Fig. 1 (a) Time evolution of the second moment m_2 and the participation number P for one disorder realization of Case I. Straight lines guide the eye for slopes 1/3 (solid line) and 1/6 (dashed line). (b) Time evolution of the finite time maximum Lyapunov exponent Λ for the trajectory of panel (a). The straight lines guide the eye for slope -1 (dashed line), which corresponds to regular motion and -0.25 (solid line).

In *Fig. 2* we compute the evolution of a part of the Lyapunov spectrum.

It is clear that the evolution of the mLE defines also the behaviour of the rest LEs.

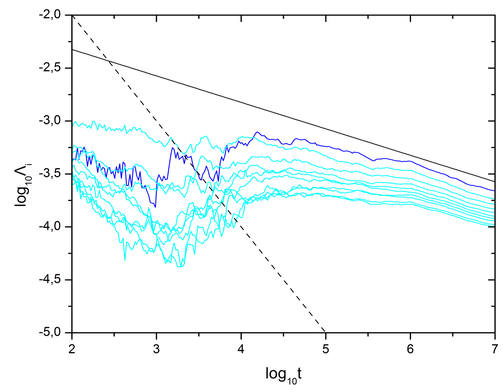

Fig. 2 The ten first LEs of a single realization of Case I. The mLE (blue line) defines the evolution of the rest LEs (cyan lines). The straight lines guide the eye for slopes -1 (solid) and -0.25 (dashed).

In order to substantiate our findings, we average $\log_{10}\Lambda$ over 50 realizations of disorder and extend our study to two more *'weak chaos'* parameter cases, namely Case II and Case III.

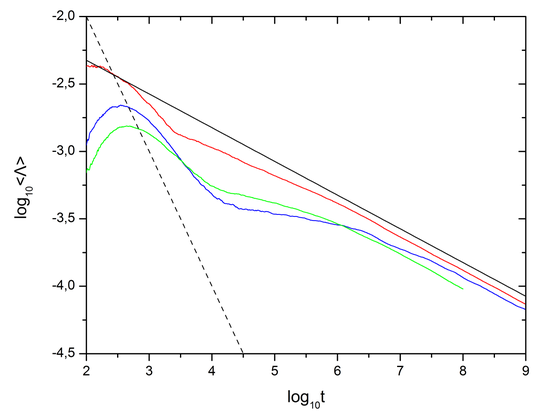

Fig. 3 Time evolution of the averaged Λ over 50 disorder realizations for the *'weak chaos'* Case I,Case II and Case III. Straight lines guide the eye for slopes -1 and -0.25.

We further differentiate the curves in *Fig. 3* following the approach used in [5, 7], estimate their slope $a_\Lambda = \frac{d(\log_{10}\Lambda(t))}{d\log_{10}t}$, and show the result in *Fig. 4*.

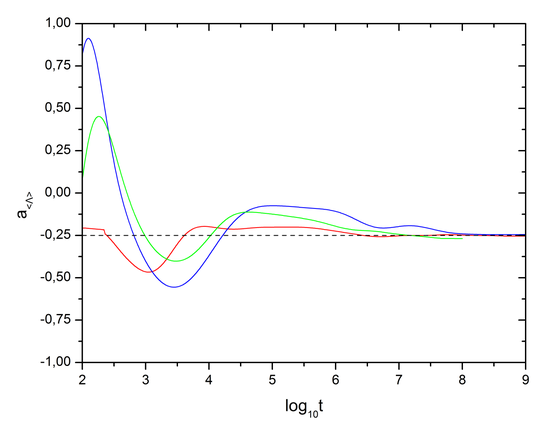

Fig. 4 Numerically computed slopes $a_{<\Lambda>}$ of the three curves of *Fig. 3*. The horizontal line denotes the value -0.25.

So far we have clear numerical proof that the dynamics inside the spreading wave packet remains chaotic up to the largest simulation times, without any tendency towards regular dynamics. To substantiate the assumptions needed for subdiffusive spreading theories, we will compare the Lyapunov time T_L defined by Λ with the time scales which characterize the subdiffusive spreading. A first time scale of this kind, T, can be obtained from the growth of the second moment $m_2 \sim t^{1/3}$. It follows that the inverse of this timescale, i.e. the effective diffusion coefficient D, is a function of the densities, and decays in time as [10]

$$\frac{1}{T} = D \sim t^{-2/3} \ , \ \Lambda \gg D \ , \ \frac{T}{T_L} \sim t^{5/12} \ . \qquad (2)$$

A second time scale can be obtained by estimating a spreading time T_s given by the increase of P by one (site), i.e. $T_s \sim 1/\dot{P}$ (with $P \sim T^{1/6}$). It follows

$$\frac{1}{T_s} \sim t^{-5/6} \ , \ \Lambda \gg \frac{1}{T_s} \ , \ \frac{T_s}{T_L} \sim t^{7/12} \ . \qquad (3)$$

As it follows from Eqs.(2,3), the dynamics remains chaotic, and the chaoticity time scale is always shorter than the spreading time scales, and especially their ratio diverges as a power law. With that we can confirm for the first time the assumption about persistent and fast enough chaoticity needed for subdiffusive spreading theories.
A second very important assumption for subdiffusive spreading theories is based on the fact that chaoticity is induced by nonlinear resonances inside the wave packet, which are the seeds of deterministic chaos and *have to meander* through the packet in the course of evolution.

A way to visualize the motion of these chaotic seeds is to follow the spatial evolution of the deviation vector used for the computation of the mLE. The energy distribution is also presented for comparison.

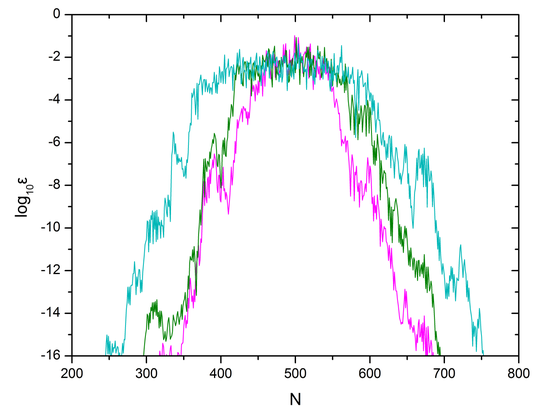

Fig. 5 Normalized energy distributions of an individual trajectory of Case I at $t = 4\times10^6$, $t = 3\times10^7$,$t = 4\times10^8$.

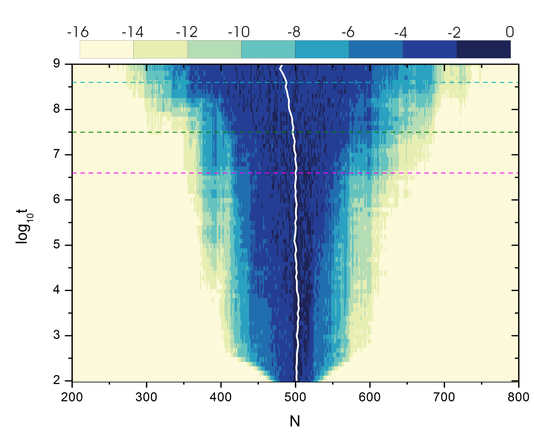

Fig. 6 The energy distribution over time. The times at which the distributions in *Fig. 5* are taken are denoted by straight horizontal lines. The white line indicates the mean position of the distribution.

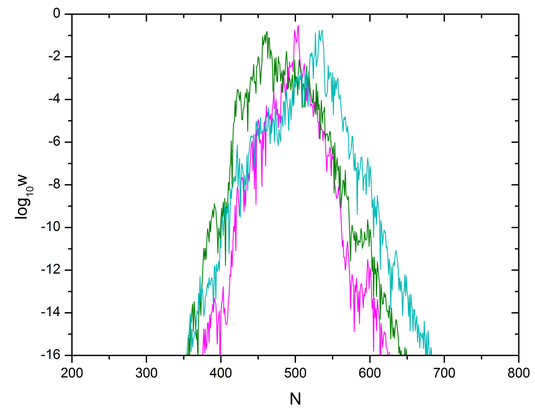

Fig. 7 Normalized deviation vector distributions of an individual trajectory of Case I at $t = 4\times10^6$, $t = 3\times10^7$,$t = 4\times10^8$.

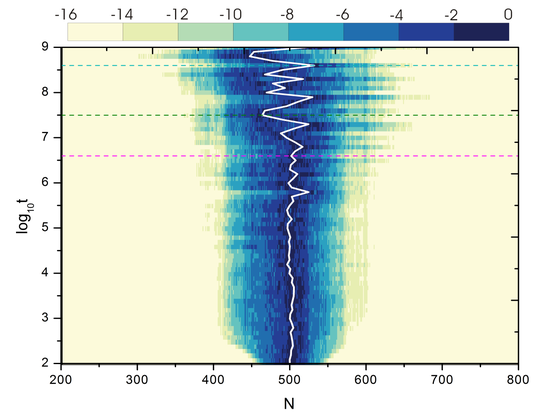

Fig. 8 The deviation vector distribution over time. The times at which the distributions in *Fig. 7* are taken are denoted by straight horizontal lines. The white line indicates the mean position of the distribution.

References

[1] P. W. Anderson, Phys. Rev. **109**, 1492 (1958).
[2] S. Flach, D. O. Krimer, and Ch. Skokos, Phys. Rev. Lett. **102**, 024101 (2009).
[3] Ch. Skokos, D. O. Krimer, S. Komineas and S. Flach, Phys. Rev. E **79**, 056211 (2009).
[4] Ch. Skokos and S. Flach, Phys. Rev. E **82**, 016208 (2010).
[5] T. V. Laptyeva, J. D. Bodyfelt, D. O. Krimer, Ch. Skokos, and S. Flach, EPL **91**, 30001 (2010).
[6] S. Flach, Chem. Phys. **375**, 548 (2010).
[7] J. D. Bodyfelt, T. V. Laptyeva, Ch. Skokos, D. O. Krimer, and S. Flach, Phys. Rev. E **84**, 016205 (2011).
[8] T. V. Laptyeva, J. D. Bodyfelt and S. Flach, EPL **98**, 6002 (2012).
[9] M. V. Ivanchenko, T. V. Laptyeva and S. Flach, Phys. Rev. Lett. **107**, 240602 (2011).
[10] T. V. Laptyeva, J. D. Bodyfelt and S. Flach, Physica D **256**, 1 (2013).
[11] Ch. Skokos, Lect. Notes Phys. **790**, 63 (2010).
[12] J. Laskar and P. Robutel, Celest. Mech. Dyn. Astron. **80**, 39 (2001).
[13] Ch. Skokos and E. Gerlach, Phys. Rev. E, **82**, 036704 (2010).
[14] E. Gerlach and Ch. Skokos, Discr. Cont. Dyn. Syst. - Ser. A, Supp., 457 (2011).